The current issue and full text archive of this journal is available at
www.emeraldinsight.com/0961-5539.htm

A robust model and numerical approach for solving solid oxide fuel cell (SOFC) problems

F. Arpino
Dipartimento di Meccanica, Strutture, Ambiente e Territorio, Università degli Studi di Cassino, Cassino, Italy
A. Carotenuto and N. Massarotti
Dipartimento per le tecnologie, Università degli Studi di Napoli "Parthenope", Naples, Italy, and
P. Nithiarasu
Civil and Computational Engineering, University of Wales Swansea, Swansea, UK

Received 20 June 2007
Revised 15 December 2007
Accepted 10 January 2008

Abstract

Purpose – The purpose of this paper is to introduce a robust mathematical model and finite element-based numerical approach to solve solid oxide fuel cell (SOFC) problems.

Design/methodology/approach – A robust mathematical model is constructed by studying pros and cons of different SOFC and other fuel cell models. The finite element-based numerical approach presented is a unified approach to solve multi-disciplinary aspects arising from SOFC problems. The characteristic-based split approach employed here is an efficient way of solving various flow, heat and mass transfer regimes in SOFCs.

Findings – The results presented show that both the model and numerical algorithm proposed are robust. Furthermore, the approaches proposed are general and can be easily extended to other similar problems of practical interest.

Originality/value – The model proposed is the first of this kind and the unified approach for solving flow, heat and mass transfer within a fuel cell is also novel.

Keywords Solid fuels, Oxide, Simulation, Porous materials, Mass, Finite element analysis

Paper type Research paper

Nomenclature

C_k = k-sepcies molar concentration (mol m^{-3})
c_p = specific heat (kJ $kg^{-1}K^{-1}$)
D_K = Knudsen diffusion coefficient ($m^2 s^{-1}$)
D_{kl} = binary diffusion coefficient ($m^2 s^{-1}$)
D^e_{km} = effective diffusion coefficient of species k in mixture m ($m^2 s^{-1}$)
D_{km} = multi-component diffusion coefficient ($m^2 s^{-1}$)
E = Nernst cell potential (V)
E_0 = standard electrode potential (V)
E_a = activation energy (kJ mol^{-1})
F_o = Forchheimer coefficient
i = current density (A m^{-2})
I = cell current (A)
I_0 = exchange current density (A m^{-2})
i_{avg} = average current density (A m^{-2})
j = species molar flux (mol $m^{-2} s^{-1}$)
K = permeability (m^2)
M_k = k-species molecular weight (kg mol^{-1})
n_e = number of transferred electrons
P = pressure (Pa)
p_k = k-species partial pressure (Pa)
r_p = average pore size (μm)

International Journal of Numerical Methods for Heat & Fluid Flow
Vol. 18 No. 7/8, 2008
pp. 811-834

0961-5539
DOI 10.1108/09615530810898971

S^e = energy source term (Jm^3s^{-1})
S_k = entropy of species k ($J\,K^{-1}$)
S_k^m = k-species mass source term ($kgm^{-2}s^{-2}$)
T = temperature (K)
$\mathbf{u}$ = velocity vector ($m\,s^{-1}$)
$\mathbf{u}_i$ = i-component of velocity vector ($m\,s^{-1}$)
V_{ki} = k-species diffusion volume
X_k = k-species molar fraction
x_i = cartesian i-coordinate (m)
y_k = k-species mass fraction

Greek
α = charge transfer coefficient
ε = porosity
η_a = activation polarization (V)
η_c = concentration polarization (V)
η_{ohm} = ohmic polarization (V)
μ_e = effective dynamic viscosity (Pa s)
ρ = fluid density ($kg\,m^{-3}$)
ρ_e = effective fluid density ($kg\,m_o^{-3}$)
σ_{kl} = diffusion collision diameter (Å)
τ_g = tortuosity
Ω_{kl} = diffusion collision integral
ϑ = time (s)
μ = dynamic viscosity (Pa s)
δ_{ij} = Kronecker delta

Constants
F = Faraday constant ($96{,}487\,C\,mol^{-1}$)
R_g = universal gas constant ($8.314\,J\,mol^{-1}\,K^{-1}$)
π = pi (3.14159)

Subscripts
f = fluid region
s = solid region
b = bulk quantities
r = reaction site quantities

Superscripts
A = anodic quantities
C = cathodic quantities

1. Introduction

The demand for energy generation has increased dramatically over the last decade, as well as the need to reduce its impact on the environment. Fuel cell technology is one of the most promising for energy generation, as it can improve energy conversion efficiency and reduce its impact on the environment. solid oxide fuel cells (SOFC), molten carbonate fuel cells, proton exchange membrane fuel cells and direct methanol fuel cells are the different types of FC that are currently being investigated in the scientific community. Among these, SOFCs are particularly promising due to the high-operating temperature, the inexpensive catalyst materials and the possibility of direct use of different fuels.

The high-operating temperature allows SOFCs to be used for cogeneration and thus this technology is suitable for stationary power generation. However, high-operating temperatures can introduce structural problems, such as thermal stresses due to different materials and different thermal expansion coefficients. Planar and tubular configurations are the two most commonly employed geomteries in the construction of SOFCs. Between the two, planar configuration presents better manufacturability. Planar configuration has recently received a great deal of attention due to its potential for higher power density.

Despite the intensive research and significant progress, SOFCs are still not ready for commercial use due to high-manufacturing costs, low-reliability and high-operating costs. To make SOFCs commercially competitive, more research effort is required to better understand some of the fundamental aspects of SOFC. To reduce cost and to increase life expectancy, some studies have been performed by reducing the operating temperature to an intermediate range below 1,073 K (Yuan and Sundén, 2005). Nowadays, numerical models play an important role in the fuel cell design and optimization. However, at present, not many robust and sound numerical solution procedures are available.

The initial and significant attempt to introduce fuel cell models date back a few years (Ferguson *et al.*, 1996; Standaert *et al.*, 1996). At the time, the computational

power available did not allow multi-dimensional transport phenomena simulation, and therefore, most of the initial models were focused on the electrochemistry. Despite the developments in of commercial computational fluid dynamic (CFD) codes, in order to overcome some of these limitations, many simplifying assumptions had to be made (Lehnert *et al.*, 2000; Yakabe *et al.*, 2000). More recently, advances in CFD techniques have allowed investigators to use multi-dimensional and multi-component models for fuel cells. These approaches have been implemented mainly using commercial codes and a single-domain approach to describe the whole fuel cell (Beale *et al.*, 2003; Autissier *et al.*, 2004; Campanari and Iora, 2004; Khaleel *et al.*, 2004; Lockett *et al.*, 2004; Lu *et al.*, 2005). Although these investigations testify a clear trend of intensive research, it is clear that a general, comprehensive and detailed numerical model for the simulation of fuel cells is still at its early stages of development (Ma *et al.*, 2005). The work undertaken by the authors aims to develop such a model based on an efficient and robust, in-house finite element code.

Fuel cells certainly represent a multi-disciplinary problem and the finite element method, currently employed in several fields of engineering (Zienkiewicz *et al.*, 2005), is appropriate for the solution of this type of problems. The numerical procedure proposed here uses a multiple-domain approach, in which the anode and cathode compartments and the electrolyte are treated separately. The characteristic-based split (CBS) algorithm (Zienkiewicz *et al.*, 2005) is used for the solution of a generalised porous medium model (Nithiarasu *et al.*, 1997; Massarotti *et al.*, 2003) that describes heat and mass transport in the free fluid and the porous medium of the anode and cathode compartments of a fuel cell. In the presented model, all the main quantities, such as for instance diffusion coefficient, current density and exchange current density, are locally calculated. The model presented here is part of a more extensive three-dimensional model for the simulation of SOFCs currently being developed by the authors. The paper is organized as follows: the next section presents the detailed mathematical model that describes fuel cell performance, Sections 3 and 4 present, respectively, the proposed numerical procedure and the CBS algorithm, Section 0 reports the results obtained for mass and energy transfer phenomena and, finally, the conclusions are drawn in the last section.

2. Governing equations

A SOFC is composed of several components and Figure 1 shows a simplified sketch of a planar SOFC. The fuel cell can be divided into following components: anodic fuel flow-channel (A), porous anode (B); catalyst layer (C); ion-conducting electrolyte (D); porous cathode (E) and oxidant flow channel (F). The electrochemical reactions taking place at the catalyst layer, represented by the thicker lines in Figure 1, generate the ionic flux through the electrolyte and the electric flux through the electrodes, the current collectors and, finally, the external load. Assuming that the cell is fed with pure hydrogen and oxygen, the electron generated by the following anodic electrochemical reaction:

$$H_2 + O^{2-} \rightarrow H_2O + 2e^-, \tag{1}$$

reaches the cathodic catalyst layer through the external load and ionizes the oxygen, according to the following electrochemical reaction:

$$\frac{1}{2}O_2 + 2e^- \rightarrow O^{2-}. \tag{2}$$

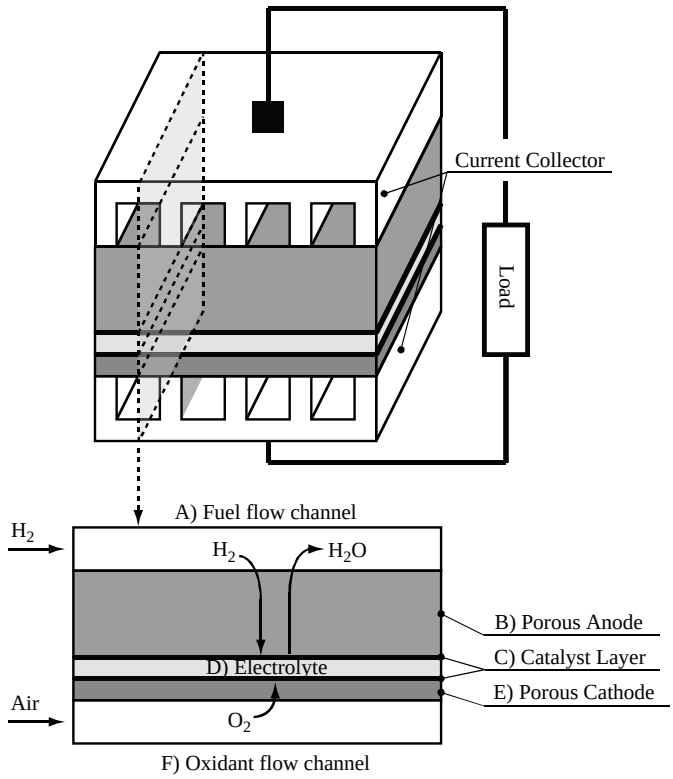

Figure 1.
Schematic representation of a planar SOFC

Under operating conditions, several phenomena (mass, energy and charge transport; chemical and electrochemical reactions) take place in different parts of the cell. These phenomena occur simultaneously and they are strictly coupled. As a consequence, to develop a better "insight" into the cell, a general, detailed and interdisciplinary mathematical model is desirable.

In principle, each phenomenon of interest in the device can be calculated through an appropriate set of partial differential equations (PDEs). The closure of the overall model is then obtained with proper relations between the different quantities involved. In the following sub-sections, the thermo-fluid dynamic and electrochemical models used in this work are presented with the closure relations. The first model allows the calculation of pressure, velocity, temperature and species concentration fields in the flow channels and the electrodes, while the second one is used for the calculation of electric quantities distribution in the device and therefore of the cell performance. In addition to the model used in the present study, the following sub-sections also summarise the other models available in literature for fuel cell simulation.

2.1 Mass and energy transfer phenomena

Over the years, many designs of SOFCs have been proposed and since the 1960s, mainly planar and tubular designs have been pursued. Conventional high-temperature SOFCs generally operate between 1,073 and 1,273 K. Lately, a number of researchers have started

focusing on intermediate temperature SOFCs (Yakabe *et al.*, 2000; Aguiar *et al.*, 2004, 2005), which typically operate between 823 and 1,073 K. Thanks to the lower operating temperatures, these devices allow a more cost-effective fabrication and better reliability. Often the positive-electrode/electrolyte/negative-electrode unit is treated as a solid component with averaged properties (Aguiar *et al.*, 2004, 2005). Such a simplification could be acceptable for very thin electrodes, as in the case of electrolyte supported devices. Nevertheless, since many researchers are focusing on electrode supported SOFCs, which can operate under 1,073 K, the presence of a thick electrode requires a detailed understanding of mass transport phenomena which drive products and reactants, respectively, to and from the reaction sites across the porous electrodes. To achieve such an objective, an appropriate mathematical model is crucial to simulate mass transfer phenomenon, which heavily influences the fuel cell performance.

The typical value of Reynolds number for SOFCs (both planar and tubular) is expected to be in the laminar range, for both the fuel and the air side. In fact, such condition is commonly assumed to be valid in the literature. However, Campanari and Iora (2004) have investigated the effective flow regime for a tubular SOFC. They have shown that even if the flow regime is laminar at the anode side, the air flow at the cathode side is closer to transition to turbulent flow. On the contrary, for a planar SOFC, Autissier *et al.* (2004) showed that the Reynolds number is 1 for the fuel side and 10 for the air side, demonstrating that the flow is laminar.

The quantities of interest in the flow channels, in the porous electrodes and in the electrolyte are described by the following advection-diffusion type equation:

$$\frac{\partial \mathbf{W}}{\partial \vartheta} + \frac{\partial \mathbf{F}_j}{\partial x_j} + \frac{\partial \mathbf{G}_j}{\partial x_j} = \mathbf{S}. \tag{3}$$

A general approach to the solution of coupled porous media and free fluid flow problems consists in the use of generalized model (Whitaker, 1961; Nithiarasu *et al.*, 1997; Massarotti *et al.*, 2001) which may be written as:

$$\mathbf{W} = \begin{pmatrix} \rho \\ \rho u_i \\ \varepsilon[(\rho c_p)_f + (1-\varepsilon)(\rho c_p)_s]T \\ \rho_e y_k \end{pmatrix} \quad \mathbf{F_j} = \begin{pmatrix} \rho u_j \\ \rho \frac{u_i u_j}{\varepsilon} + \varepsilon p \delta_{ij} \\ (\rho c_p)_f u_j T \\ u_j \rho_e y_k \end{pmatrix} \mathbf{G_j} = \begin{pmatrix} 0 \\ -\mu_e \frac{\partial u_i}{\partial x_j} \\ -k_e \frac{\partial T}{\partial x_i} \\ -\rho_e D^e_{km} \frac{\partial y_k}{\partial x_j} \end{pmatrix}, \tag{4}$$

and with the source term:

$$\mathbf{S} = \begin{pmatrix} 0 \\ \frac{\mu \varepsilon u_i}{K} + \frac{\rho F_o \varepsilon^2 |\mathbf{u}|}{\sqrt{K}} \\ S^e \\ S^m_k \end{pmatrix}. \tag{5}$$

The subscript e for density and viscosity in equation (4) indicates the *effective* quantity in the porous domain (Massarotti *et al.*, 2001). The same set of equations can then be

used for the calculation of the quantities of interest in both the free fluid region ($\varepsilon = 1; K \rightarrow \infty$) and in the porous domain ($0 < \varepsilon < 1; 0 < K < \infty$) by just changing the properties of the medium considered (effective property → fluid property). The right hand side (RHS) includes the source/sink terms S_k^m and S^e in the species and energy conservation equations, that are derived from chemical and electrochemical reactions. Such terms take into account both the steam reforming reactions in the fuel channel and the electrochemical reactions at the catalyst layer. More details about the source terms are given in the next section.

Since different components have different functions, a straightforward way of modelling the fuel cells is to treat each component independently. Nevertheless, such a separated domain approach generates interfaces, at the two sides of which chemical and physical boundary conditions must be coupled and a considerable effort is required to define appropriate interface boundary conditions.

Since the described set of PDEs is difficult to directly solve, a variety of different approaches and simplifications have been proposed by different authors over the last ten years. One critical aspect is the computational effort required to achieve a desired level flow field resolution. In fact, the presence of very large source-sink terms in the momentum conservation equation requires a very stable numerical solution algorithm. To overcome this difficulty, various approaches have been proposed in literature. Many authors decouple the free fluid channel from the porous electrode. In the electrode-field, some authors assume that the velocity is linked to pressure field via the Darcy equation (Larrian *et al.*, 2004; Lin and Beale, 2006). It should be noted that in such situations, an appropriate interfacial condition between free fluid in the channel and porous electrode should be specified (Vafai and Kim, 1990; Vafai, 2000). The Darcy model cannot predict the viscous effect and the flow development. It also breaks down when flow velocity is not small, which is the case when the inertial forces are not negligible. Some other simplifications proposed in literature neglect the velocity field in the porous electrode and assume a pure diffusive behaviour for species concentration field, according to Fick's law (Aguiar *et al.*, 2004; Campanari and Iora, 2004):

$$j_k = -D_{km}^e \frac{\partial C_k}{\partial x_i}. \tag{6}$$

The above species fluxes are also related to the current density according to the well-known Faraday's law (Singhal and Kendall, 2003):

$$j_k = \frac{i}{n_e F}. \tag{7}$$

Some authors completely neglect the presence of the porous electrode assuming that the electrodes are very thin (Suwanwarangkul *et al.*, 2006). In this case, the above gradient across the porous electrodes is neglected and the fluxes of reactants and products due to electrochemical reactions are directly calculated according to equation (7).

Table I presents a summary of above discussed common modelling approaches to the solution of thermo-fluid dynamic aspects in SOFCs. Basically, all the models available in literature could be seen as a simplification of the generalized model. Even though such simplifications significantly reduce the computational requirements, they can also introduce errors in the final solution. In the present study, the authors do not use any of such simplifying assumptions.

Table I.
Summary of common assumptions and modelling techniques available in the literature for the fluid-dynamic aspects of SOFCs

Model	**W**	**F**	**G**	**S**	References
Free fluid channel					
Navier-Stokes equations	$\begin{pmatrix} \rho \\ \rho u_i \\ (\rho c_p)_f T \\ \rho y_k \end{pmatrix}$	$\begin{pmatrix} \rho u_j \\ \rho \frac{u_i u_j}{\varepsilon} + p\delta_{ij} \\ (\rho c_p)_f u_j T \\ u_j \rho y_k \end{pmatrix}$	$\begin{pmatrix} 0 \\ -\mu \frac{\partial u_i}{\partial x_j} \\ -k \frac{\partial T}{\partial x_i} \\ -\rho D^e_{km} \frac{\partial y_k}{\partial x_j} \end{pmatrix}$	$\begin{pmatrix} 0 \\ 0 \\ S^e \\ S^m_k \end{pmatrix}$	Campanari and Iora (2004), Khaleel *et al.* (2004), Lu *et al.* (2005), Lin and Beale (2006), Lu and Schaefer (2006) and Suwanwarangkul *et al.* (2006)
Plug flow	$\begin{pmatrix} \rho \\ \rho u_i \\ (\rho c_p)_f T \\ \rho y_k \end{pmatrix}$	$\begin{pmatrix} 0 \\ 0 \\ (\rho c_p)_f u_j T \\ u_j \rho y_k \end{pmatrix}$	$\begin{pmatrix} 0 \\ 0 \\ -k \frac{\partial T}{\partial x_i} \\ -\rho D^e_{km} \frac{\partial y_k}{\partial x_j} \end{pmatrix}$	$\begin{pmatrix} 0 \\ 0 \\ S^e \\ S^m_k \end{pmatrix}$	Larrian *et al.* (2004)
Channel flow field neglected	–	–	–	–	Aguiar *et al.* (2004), Greene *et al.* (2006) and Inui *et al.* (2006)
Porous electrode					
Darcy	$\begin{pmatrix} \rho \\ \rho u_i \\ (\rho c_p)_f T \\ \rho y_k \end{pmatrix}$	$\begin{pmatrix} \rho u_j \\ p\delta_{ij} \\ (\rho c_p)_f u_j T \\ u_j \rho y_k \end{pmatrix}$	$\begin{pmatrix} 0 \\ 0 \\ -k \frac{\partial T}{\partial x_i} \\ -\rho D^e_{km} \frac{\partial y_k}{\partial x_j} \end{pmatrix}$	$\begin{pmatrix} 0 \\ \frac{\mu}{K} u_i \\ S^e \\ S^m_k \end{pmatrix}$	Lin and Beale (2006)
Pure diffusive field: Fick's law	–	$\begin{pmatrix} 0 \\ 0 \\ 0 \\ 0 \end{pmatrix}$	$\begin{pmatrix} 0 \\ 0 \\ -k \frac{\partial T}{\partial x_i} \\ -\rho D^e_{km} \frac{\partial y_k}{\partial x_j} \end{pmatrix}$	$\begin{pmatrix} 0 \\ 0 \\ S^e \\ \frac{i}{n_e F} + S^m_k \end{pmatrix}$	Aguiar *et al.* (2004) and Campanari and Iora (2004)
Electrode fields neglected	–	–	–	–	Suwanwarangkul *et al.* (2006)

Species diffusion coefficient D^{e}_{km} calculation procedure is crucial for an accurate estimation of species concentrations. In the absence of experimental data, several models have been proposed in literature for the calculation of binary species diffusion coefficients. The most common method for theoretical estimation of gaseous diffusion is that developed independently by Chapman and Enskog (Cussler, 1997; Perry *et al.*, 1997), which is based on a detailed analysis of molecular motion in dilute non-polar gases. Other correlations, such as for instance the Fuller-Shcettler-Giddings equations, are derived on the basis of experimental and empirical data (Cussler, 1997; Perry *et al.*, 1997). In Table II, species binary diffusion models are given together with some of the authors who have used them for the simulation of SOFC. The effect of the presence of the porous electrode is often taken into account through the Knudsen diffusion coefficient (Zhu and Kee, 2003):

$$D_K = \frac{4}{3} r_p \sqrt{\frac{8R_g T}{\pi M_i}}. \tag{8}$$

Therefore, the effective diffusion coefficient of species k in mixture m, used in the present study is given by the following relation:

$$\frac{1}{D^{e}_{km}} = \frac{\tau_g}{\varepsilon} \left(\frac{1}{D_{km}} + \frac{1}{D_K} \right). \tag{9}$$

Since other effects, such as Knudsen diffusion are likely to be present, and the exact nature of tortuosity is unclear, the tortuosity factor τ_g is generally used merely as a phenomenological fitting parameter (Zhao and Virkar, 2005).

2.2 Electrochemistry

Fuel cells are electrochemical devices in which energy conversion is based on anodic and cathodic electrochemical reactions according to equations (1) and (2), respectively. Assuming that the fuel cell is supplied with pure hydrogen and oxygen, the ideal electromotive force associated with electrochemical reactions is given by Nernst equation (Singhal and Kendall, 2003):

Model/value	Equation	Error (per cent)	References
Chapman-Enskog	$D_{kl} = 1.86 \times 10^{-3} \frac{T^{3/2} \left(\frac{1}{M_k} + \frac{1}{M_l} \right)^{0.5}}{p \sigma^2_{kl} \Omega_{kl}}$	7.3	Yakabe *et al.* (2000)
Fuller-Shcettler-Giddings	$D_{kl} = 10^{-3} \frac{T^{1.75} \left(\frac{1}{M_k} + \frac{1}{M_l} \right)^{0.5}}{p \left[\left(\sum_i V_{ik} \right)^{1/3} + \left(\sum_i V_{il} \right)^{1/3} \right]^2}$	5.4	Campanari and Iora (2004)
Constant over the domain	–		Lin and Beale (2006)

Table II.
Summary of common models employed for species binary diffusion coefficient

Sources: Cussler (1997), Perry *et al.* (1997)

$$E = E_0 - \frac{R_g T}{2F} \ln\left(\frac{p_{H_2O}}{p_{H_2} p_{O_2}^{0.5}}\right). \tag{10}$$

Under operating conditions, the cell voltage is lower than the Nernst voltage due to the losses (or over-potentials), mainly activation, concentration and ohmic over-potentials. Thus, the effective potential may be calculated as:

$$V = E - \eta_a - \eta_c - \eta_{ohm}. \tag{11}$$

Activation losses are related to the activation energy required by the chemical reactions. Assuming a single rate controlling reaction, the relation between current density and charge transfer over-potential is governed by phenomenological Butler-Volmer equation (Singhal and Kendall, 2003), which represents the net anodic and cathodic current density due to an electrochemical reaction:

$$i = i_0 \left[\exp\left(\alpha^A \frac{n_e F \eta_a}{R_g T}\right) - \exp\left(-\alpha^C \frac{n_e F \eta_a}{R_g T}\right)\right]. \tag{12}$$

The exchange current density i_0 at the electrode/electrolyte interface, which appears in the above equation, is not a simple constant parameter. In fact, its value depends not only on the operating conditions and material properties, but also on fuel cell electrochemical reaction kinetic and reactants/products concentrations (Celik *et al.*, 2005). Even though many authors assume the exchange current density to be constant, a general expression of such parameter relates it to the absolute temperature, according to the following Arrhenius type equation:

$$i_0 = k_0 \exp\left(-\frac{E_a}{RT}\right). \tag{13}$$

The factor k_0 and the activation energy E_a are usually determined using empirical relations developed on the basis of reaction kinetics. Table III gives some of the models and relations available in literature for estimation of the exchange current density. Another possibility for estimating exchange current density is by fitting the experimental results, which lumps the effect of electrode microstructure on the reaction kinetics; an example of such technique is available in Chan and Xia (2002).

When the fuel cell is under no load (open circuit), the species concentrations at the reaction sites are the same as in the bulk channel flow. Under normal operating conditions (closed circuit), a concentration gradient across the electrode structures induces concentration fluxes as a result of fuel and oxidant consumption at the reaction site. The difference in concentration between the flow channel and the reaction site is directly related to the concentration losses. These losses can be evaluated as the difference between the Nernst potential in the bulk flow channel and the same quantity in the reaction sites according to the following relation (EG&G, S.P. Inc., 2000; Chan *et al.*, 2001; Zhu and Kee, 2003; Aguiar *et al.*, 2004; Campanari and Iora, 2004; Greene *et al.*, 2006):

$$\eta_c = \eta_c^A + \eta_c^C = \frac{R_g T}{2F} \ln\left(\frac{X_{H_2}^b X_{H_2O}^r}{X_{H_2}^r X_{H_2O}^b}\right) + \frac{R_g T}{4F} \ln\left(\frac{X_{O_2}^b}{X_{O_2}^r}\right). \tag{14}$$

Table III.
Examples of models and relations available in the literature for the exchange current density i_0 estimation

Model	$\mathbf{k_0}$		$\mathbf{E_a}$ (kJ/mol)		$\mathbf{i_0}$ (A/m^2)		References
	Anode	Cathode	Anode	Cathode	Anode	Cathode	
(13)	$7\times10^9\frac{p_{H_2}p_{H_2O}}{p_{ref}^2}$	$7\times10^9\frac{p_{O_2}}{p_{ref}}$	110	120			Campanari and Iora (2004)
	$\frac{RT}{3F}6.2\times10^{11}\left(\frac{p_{H_2O}}{K_{eq,H_2}p_{H_2}}\right)^{0.266}$	$0.25\times10^{10}\cdot RT\cdot p_{O_2,cat}^{0.5}$	120	130			Suwanwarangkul *et al.* (2006)
	$\frac{RT}{2F}2.35\times10^{11}$	$\frac{RT}{2F}6.54\times10^{11}$	140	137			Aguiar *et al.* (2004)
	$\frac{RT}{3F}125.6\times10^{10}\cdot p_{O_2,anode}^{0.15}$	$\frac{RT}{4F}62.7\times10^6 p_{O_2,cathode}^{0.5}$	138	136			Suzuki *et al.* (2005)
Constant i_0					5,300	2,000	Li and Chyu (2003)
					6,300	3,000	Ji *et al.* (2006)
					0.2		Lu *et al.* (2005)
					Experiments		Greene *et al.* (2006)

Diffusion phenomena influence the cell limiting current, which corresponds to zero reactant concentration at the reaction site. Instead of using equation (14), some authors calculate the concentration polarization based on the limiting cell current, assuming a constant value of the diffusion coefficient (Khaleel *et al.*, 2004; Lu *et al.*, 2005). However, it is evident from recent results that the concentration losses depends strictly on the reactant utilization factor (Sundén and Faghri, 2005) and electrode thickness. Since oxidant utilization factor is usually much lower than fuel utilization factor, cathodic concentration losses are usually smaller in comparison to anodic ones. Nonetheless, for electrolyte- and cathode-supported fuel cells, the anodic concentration polarization can become very small since the anode is very thin. On the basis of these considerations, some authors completely neglect the concentration polarization effects (Chan and Xia, 2002; Larrian *et al.*, 2004; Lin and Beale, 2006; Nishino *et al.*, 2006).

The ohmic losses are due to the resistance to the ion flow in the electrolyte and due to the resistance to the electron flow in the electrodes. Since the electric current flow in both electrodes and electrolyte obeys the Ohm's law, ohmic losses can be expressed by:

$$\eta_{\text{ohm}} = I \cdot R_i, \tag{15}$$

where R_i represents the overall resistance, that is the sum of the cathode, electrolyte, anode, interconnect and contact ohmic resistances. The main contribution to the value of R_i is due to the electrolyte resistance and decreases when the operating temperature increases (Singhal and Kendall, 2003). Typically, ohmic resistivities are calculated on the basis of empirical formula of the type:

$$R_i = A \cdot \exp\left(\frac{B}{T}\right). \tag{16}$$

Values of specific resistance of both tubular and planar configuration of SOFC can be found in the literature (Li and Chyu, 2005; Stiller *et al.*, 2005; Nishino *et al.*, 2006).

The electrochemical reactions taking place in the fuel cell together with activation and ohmic losses are responsible for the heat generation within the device. Assuming the energy source term as a flux at the catalyst layer, it is described by the following:

$$\dot{q} = \frac{T \cdot i}{2F}(S_{\text{H}_2\text{O}} - S_{\text{H}_2} - 2S_{\text{O}_2}) + i(\eta_a + \eta_{\text{ohm}}), \tag{17}$$

where the first term in RHS of equation (17) represents the anodic and cathodic reversible heat generation per unit of area, while the last term is the irreversible heat flux due to electrochemical reactions (Singhal and Kendall, 2003; Ma *et al.*, 2005).

3. Proposed solution approach

The fuel cell is divided into three computational domains:

(1) anodic compartment, including the flow channel, electrode and catalyst layer;

(2) electrolyte domain; and

(3) cathodic compartment (Figure 1).

Since the thickness of the catalyst layer, where chemical reactions occur, is at least two orders of magnitude smaller than the other parts of the domain, this is assumed simply

to be a surface between porous electrode and electrolyte. Appropriate PDEs can be solved iteratively for different domains in order to predict the distribution of the quantities of interest. The link between the different domains is then obtained imposing appropriate interface boundary conditions.

In order to realize a numerically tractable model of a complete fuel cell the following assumptions have been invoked:

- the gases in the mixture are assumed to behave as ideal gases;
- the flow is assumed to be laminar; and
- anode and cathode are modelled as saturated porous media of constant porosity.

The aim of the proposed paper is to investigate the mass and energy transport phenomena in the anodic and cathodic compartments of a SOFC. In order to achieve such goal, a generalised model is employed to describe the flow through the porous electrodes. According to general advection-diffusion type equation (3), the proposed mathematical model is constituted by the terms given in equations (4) and (5). In the absence of experimental data, the binary diffusion coefficients have been estimated according to the Chapman-Enskog theory, as illustrated in Table II. The effective porous medium diffusion coefficient of species k in mixture m is calculated according to equations (8) and (9). The fuel cell performance is predicted in terms of operative voltage according to equations (10)-(16). In particular, the Butler-Volmer equation (12) has been solved by assuming both transfer coefficients α_a and α_c equal to 0.5, and employing the relations and the parameters available in Campanari and Iora (2004) (Table III) to predict the anodic and cathodic exchange current densities. The concentration polarization is calculated as the difference of Nernst voltage in the bulk channel and the same quantity calculated at the reaction site, according to equation (14). The ohmic losses have been evaluated on the basis of the average current density, according to equation (15). Finally, the heat generation has been modelled as energy fluxes at the catalyst and has been calculated according to equation (17).

The overall calculation procedure starts form the anodic compartment by solving the generalised model. The species and energy equations are solved using the mass and energy source/sink terms as a Neumann boundary condition at the catalyst layer, calculated on the basis of local current density distribution. The local current density distribution at the interface between electrode and electrolyte is calculated by solving the Butler-Volmer equation, and the local value of current density allows the calculation of species and energy fluxes at the catalyst layer according to equations (7) and (17). The anodic calculation starts with guessing an initial local current density distribution and a local subdivision coefficient of the heat flux between anodic compartment and electrolyte. Once convergence is obtained for the anodic compartment, the calculation procedure moves to the electrolyte section and then to the cathodic compartment. The continuity of temperature at the interface between different domains requires an overall iterative process in order to calculate the effective subdivision coefficient of the energy flux at the anodic compartment. In particular, the overall convergence is assumed when no differences in temperature are observed at the interface between the domains.

4. The characteristic-based split algorithm

A 2D finite element code based on the CBS algorithm was developed to solve the equations employed in the presented model. The CBS procedure has been the subject of research for the last ten years and it has been applied for the solution of many problems, from fluid dynamics and heat transfer to solid mechanics (Nithiarasu, 2003; Nithiarasu *et al.*, 2004; Zienkiewicz *et al.*, 2005; Massarotti *et al.*, 2006). The CBS algorithm is based on the temporal discretization of the flow equations along the characteristics, and on the split of the operator in order to obtain pressure stabilization in the solution of incompressible flows. Briefly, the characteristic procedure is based on particle backtracking in time-space domain, avoiding the need to resort to moving coordinates. Such approach is made possible by employing a temporal Taylor expansion. The obtained backward approximation results in extra, consistent, second-order stabilizing terms which suppress the oscillations generated from the discretization of the convective terms.

The momentum equation introduced in the generalized model is a typical convection-diffusion equation and can therefore be discretized in time using the characteristic process. In particular, the time-discrete momentum equation can be written as (Massarotti *et al.*, 2003):

$$\mathbf{u}^{n+1} + \theta_1 \varepsilon \Delta\vartheta P\mathbf{u}^{n+1} = \mathbf{u}^n + \varepsilon\Delta\vartheta\Big[-(\nabla p)^{n+\theta_2} - \nabla\Big(\frac{\mathbf{u}\cdot\mathbf{u}}{\varepsilon^2}\Big)^n + \frac{\mu_e}{\rho\varepsilon}(\nabla^2\mathbf{u})^n + \mathbf{S}^n - (1-\theta_1)P\mathbf{u}^n\Big], \tag{18}$$

where $0.5 \le \theta_1 \le 1$ and $0 \le \theta_2 \le 1$. The pressure term in equation (18) is not treated explicitly, but is evaluated at a time $\vartheta^n + \theta_2\Delta\vartheta$ and is given by:

$$(\nabla p)^{n+\theta_2} \equiv \theta_2(\nabla p)^{n+1} + (1-\theta_2)(\nabla p)^n, \tag{19}$$

while the terms:

$$P = \frac{\mu_e\varepsilon}{\rho K} + \frac{F_0\varepsilon|\mathbf{u}|}{\sqrt{K}}, \tag{20}$$

and:

$$\mathbf{S} = \frac{\Delta\vartheta}{2}\mathbf{u}\cdot\nabla\Big[-\nabla\Big(\frac{\mathbf{u}\cdot\mathbf{u}}{\varepsilon}\Big) + \mathbf{u}\cdot\nabla(-\nabla p)\Big], \tag{21}$$

represent, respectively, the porous term and the stabilizing term coming out form the discretization procedure. In the present study, it is assumed that $\theta_1 = 0$ and $\theta_2 = 1$ and therefore the semi-implicit form of the CBS is employed for the generalised model (Massarotti *et al.*, 2006). Taking all terms due to the porous matrix to the left hand side of the equation, the first step of the CBS algorithm is the calculation of an intermediate velocity $\tilde{\mathbf{u}}$ from the momentum equation without including the pressure term:

$$\tilde{\mathbf{u}}^{n+1} = \mathbf{u}^n + \varepsilon\Delta\vartheta\Big[-\nabla\Big(\frac{\mathbf{u}\cdot\mathbf{u}}{\varepsilon^2}\Big) + \frac{\mu_e}{\rho\varepsilon}(\nabla^2\mathbf{u}) + \frac{\Delta\vartheta}{2}\mathbf{u}\cdot\nabla\Big(-\nabla\Big(\frac{\mathbf{u}\cdot\mathbf{u}}{\varepsilon}\Big)\Big) + P\mathbf{u}\Big]^n. \tag{22}$$

The second step is the calculation of the pressure from a modified Poisson type equation, which ensures the continuity equation to be satisfied, and for the generalised model can be written as:

$$\nabla^2 p^{n+1} = \nabla\left(\frac{\tilde{\mathbf{u}}^{n+1}}{\varepsilon\Delta\vartheta}\right). \tag{23}$$

Finally, the corrected velocities can be obtained, once the pressure is known, in the third step of the algorithm, written as:

$$\mathbf{u}^{n+1} - \tilde{\mathbf{u}}^{n+1} = \varepsilon\Delta\vartheta\left[-\nabla p + \frac{\Delta\vartheta}{2}\mathbf{u}\cdot\nabla(-\nabla p)\right]^n. \tag{24}$$

Once the flow field is determined, it is possible to solve the energy and the species conservation equations, which are explicitly discretized in time as follows:

$$\frac{T^{n+1} - T^n}{\Delta\vartheta} = \frac{\left[-(\rho c_p)_f \nabla\cdot\mathbf{u}T + k_e\nabla^2 T\right]^n}{\left[(\rho c_p)_f + (1-\varepsilon)(\rho c_p)_s\right]} + \frac{\Delta\vartheta}{2}\,\frac{\mathbf{u}\cdot\nabla\left[(\rho c_p)_f\nabla\cdot(\mathbf{u}T)\right]^n}{\left[(\rho c_p)_f + (1-\varepsilon)(\rho c_p)_s\right]}, \tag{25}$$

$$\frac{\rho_e\left(y_k^{n+1} - y_k^n\right)}{\Delta\vartheta} = \left[-\rho_e\nabla\cdot(\mathbf{u}y_k) + \rho_e D_{km}^e\nabla^2 y_k\right]^n + \frac{\Delta\vartheta}{2}\mathbf{u}\cdot\nabla[\rho_e\nabla\cdot(\mathbf{u}y_k)]^n. \tag{26}$$

The resulting equations are discretized in space using a standard Galerkin finite element procedure (Zienkiewicz and Taylor, 2000; Lewis *et al.*, 2004). The computational domain is then subdivided into a triangular mesh of finite elements. Within the elements each variable is approximated by a linear function, that can be expressed in terms of its value at the three nodes of the element:

$$\phi = \sum_{n=1}^{3} N_n\bar{\phi}_n, \tag{27}$$

where N_n is the shape function and $\bar{\phi}_n$ is the value of the generic approximated variable ϕ at node n. The equations obtained substituting the approximated function in equations (22)-(26) are then weighted using the same shape function, N_n, and integrated over the whole domain.

The discretized equations can be solved in both the anodic and cathodic compartments, to derive the quantities of interest to evaluate the fuel cell performances. The steps of the proposed solution procedure are listed below, starting from anodic compartment:

(1) imposition of boundary conditions and guess initial solution;

(2) calculation of local current density distribution at the anodic compartment by solving the Butler-Volmer equation;

(3) calculation of species and energy fluxes within the anodic compartment;

(4) guess distribution of energy flux between anodic compartment and electrolyte;

(5) solve transport equation for momentum, energy and species within the anodic compartment;

(6) the energy flux and the temperature distribution at the interface between anodic compartment and electrolyte represent the required interface conditions for the solution of energy equation within the electrolyte;

(7) the energy flux at the interface between electrolyte and cathodic compartment represents the required interface condition for the solution of energy equation resolution within the cathodic compartment;

(8) calculation of local current density distribution within the cathodic compartment by solving the Butler-Volmer equation;

(9) calculation of species fluxes within the cathodic compartment;

(10) solve transport equation for momentum, energy and species within the cathodic compartment;

(11) temperature distribution at the interface between electrolyte and cathodic compartment must be the same to satisfy continuity; if not, restart from step 2 until convergence is reached;

(12) Nernst equation solution and concentration overpotentials calculation; and

(13) overall cell performance prediction.

5. Numerical results

The proposed model has been verified by simulating mass and energy transfer phenomena in a planar anode-supported SOFC, for which some experimental data are available in literature (Yakabe *et al.*, 2000). Figure 2 shows the computational domains and the boundary conditions employed for the anodic and cathodic compartments. At the inlet sections of the anodic/cathodic domain, a mixture of assigned species concentration values with given velocity and temperature are assumed to enter the domain. At the exit of the domain free boundary conditions are assumed for the quantities of interest. No-slip velocity and adiabatic conditions are imposed on all other sides of the domain, which are also considered to be impermeable to the species in the mixture. Assuming that the cell is supplied with hydrogen and air, the species mass fluxes at the catalyst layer are expressed by the following equations:

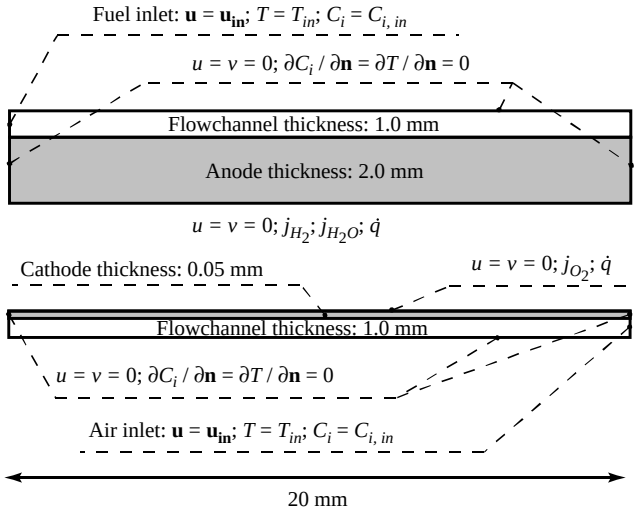

Figure 2.
Domain definitions and boundary conditions employed for the simulation of the anodic compartment (top) and the cathodic compartment (bottom) of an anode supported SOFC

$$j_{H_2} = -\frac{M_{H_2} i}{2F};\ j_{H_2O} = \frac{M_{H_2O} i}{2F};\ j_{O_2} = -\frac{M_{O_2} i}{4F}. \quad (28)$$

Since the generalized model is employed to describe the flow through the porous electrode, no further interface conditions are required between free fluid and porous domain (Vafai and Kim, 1990; Massarotti *et al.*, 2001). The anodic parameters adopted for the simulation, according to the structural nature of the electrode, are listed in Table IV. As the same parameters are not available for the cathode, the quantities listed in Table IV have been employed for both the electrodes. This assumption is not expected to affect the results adversely, as the thickness of the cathode is very small compared to the anode. The temperature gradient across the electrolyte is assumed to be negligibly small due to the fact that electrolyte layer is two orders of magnitude thinner than the anode. As a consequence, the anodic and cathodic temperature distributions at the catalyst layer must be the same. This is achieved as follows. At each time step the activation polarization and the new local current density distribution are calculated by solving the Butler-Volmer equation (12) as a function of local pressure and species molar fraction distribution at the catalyst layer. The local current density is then used in equation (17) to calculate the heat flux that is applied between anodic and cathodic catalyst layers to obtain the same temperature distribution profile at the interface. As mentioned in the previous section, this is achieved via an iterative procedure. The rest of the calculation follows the steps listed in the previous section.

The simulations have been performed by employing structured triangular grids with 2,916 nodes and 5,600 elements for both the anodic and cathodic compartments (Figure 3). The computational grids shown in Figure 3 have been chosen after a careful mesh sensitivity analysis performed for both compartments.

Table IV.
List of parameters employed for the electrode modelling

Porosity ε	Tortuosity τ_g	Average pore size r_p (μm)	Permeability of the anode ($m^2Pa^{-1}s^{-1}$)
0.46	4.5	2.6	1.7×10^{-10}

Source: Yakabe *et al.* (2000)

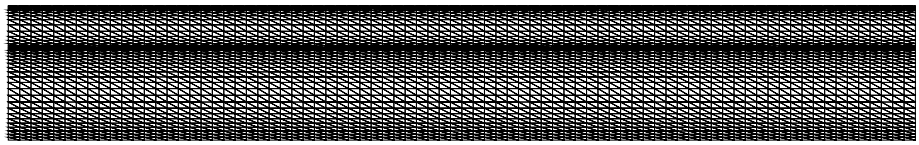

Anodic computational grid: 2,916 nodes and 5,600 triangular elements.

Cathodic computational grid: 2,916 nodes and 5,600 triangular elements.

Figure 3.
Grids employed for numerical simulation of the anodic compartment of an anode supported SOFC

In order to verify the proposed model against available experimental data (Yakabe *et al.*, 2000), the anodic compartment has been supplied with a ternary mixture of H_2, H_2O and Ar. To reproduce the experimental conditions, isothermal conditions are assumed by keeping the domain temperature constant at 1,023 K. The fuel is assumed to enter the anode at a constant velocity of 2.0 m/s and the mass flow rate ratio between H_2 and H_2O at the inlet is kept at 0.8. These inlet conditions ensure that the fuel utilization factor is lower than 5 per cent, which represents the experimental condition. Also, the ideal Nernst voltage is kept constant to reproduce the experimental conditions. The inlet hydrogen concentration is varied by varying the argon concentration in the inflow mixture.

Figure 4 shows the concentration polarization difference between a mixture containing argon $\left(\eta_c^A\right)$ and a mixture with no argon $\left(\eta_{c0}^A\right)$. The results shown in Figure 4 are for an average current density value of 0.3 and 0.7 A/cm^2. At 0.3 A/cm^2, the present numerical solution agrees excellently with the experimental data. At $i_{avg} = 0.7$ A/cm^2, however, the proposed model slightly under predicts the experimental data when the fuel is highly diluted with argon. Compared to the values predicted with the presented procedure, the numerical results of Yakabe *et al.* (2000) present a larger deviation from the experimental data at almost all fuel concentration values considered. It is interesting to notice that the numerical results of Yakabe *et al.* (2000) have been obtained by assuming a constant value of current density distribution at the catalyst layer, while the results from the present model have been obtained by locally calculating the current density value at the catalyst layer according to equation (12).

To evaluate the effect of using a variable current density, another case with isothermal conditions (1,023 K) is simulated. To maintain a fuel utilization factor between 5 per cent at $i_{avg} = 0.1$ A/cm^2 and 50 per cent at $i_{avg} = 1.0$ A/cm^2, the fuel inlet

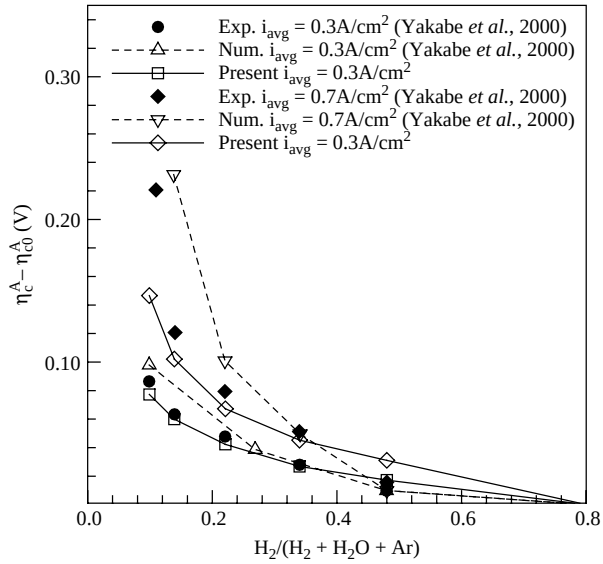

Source: Yakabe *et al.* (2000)

Figure 4.
Concentration overpotentials at $i_{avg} = 0.3$ and $i_{avg} = 0.7$ A/cm^2 for an Argon diluted fuel: comparison with the experimental and numerical data available from literature

velocity is set to 8.45×10^{-2} m/s, while the air inlet velocity assumed is 1.0 m/s. Figure 5 shows the hydrogen and oxygen molar fraction distributions in the anodic and cathodic compartments, calculated for both constant current density value (top) and locally calculated current density distribution (bottom) with a mean current density value equal to 0.3 A/cm^2. The mean effective diffusion coefficient of hydrogen calculated in the porous electrode is 1.38×10^{-5} m^2/s. However, Figure 5 clearly shows that the diffusion process is different in the two cases studied, particularly in the anodic compartment, where the two hydrogen distributions differ significantly at the interface. Figure 6 shows the anodic current density distribution at the catalyst layer. As seen the maximum local current density value is obtained at the inlet section. It is also noticed that the difference between maximum and minimum local current density values increases as the mean current density value increases.

The effects of using constant or locally calculated current density distribution are more clearly shown in Figure 7. Here, the cell polarizations are plotted against the mean current density. The figure on the left shows the results for a constant current density assumption and the one on the right shows the results for locally distributed current density at the catalyst layer. These figures show a significant difference in both concentration and activation losses at the anodic compartment. This is clearly due to the thickness of the anode being much bigger than that of the cathode. Also, from Figure 7 it is clear that the local current density distribution influences the species molar fraction distribution in the anodic compartment. In fact, the local distribution of the current density (Figure 6) produces a more homogeneous hydrogen molar fraction distribution at the catalyst layer than the one obtained with a constant current density assumption. As a result, the activation and concentration losses in the anode are lower when variable current density is assumed. As a consequence, the fuel cell shows a better performance with a variable current density assumption in terms of both operative voltage and power density, as shown in Figure 8. This figure shows that at

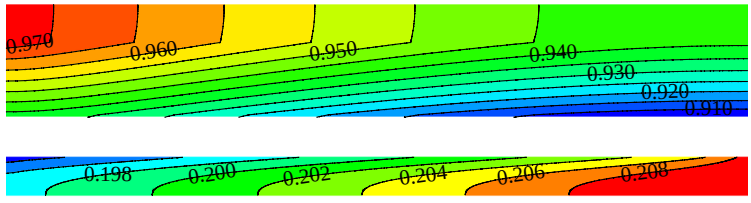

Hydrogen mole fraction (top) and oxygen mole fraction (bottom), $i(x) = i_{avg}$.

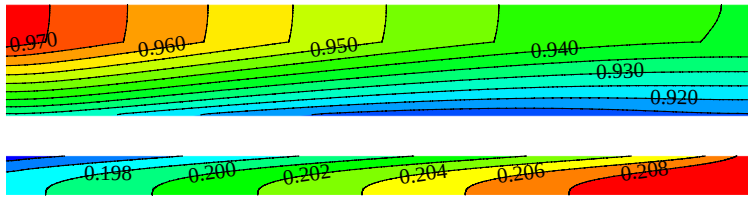

Hydrogen mole fraction (top) and oxygen mole fraction (bottom), $i(x) = f(x)$

Figure 5.
Hydrogen and oxygen molar fraction distributions obtained with a constant current density (top) and locally calculated current density (bottom) distributions at the catalyst layer for a mean current density value $i_{avg} = 0.3$ A/cm^2

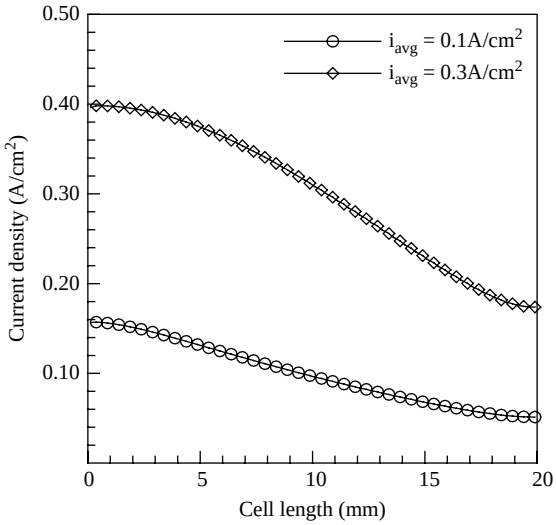

Figure 6.
Anodic current density distribution at the catalyst layer for mean current density values $i_{avg} = 0.1$ and $i_{avg} = 0.3\ A/cm^2$

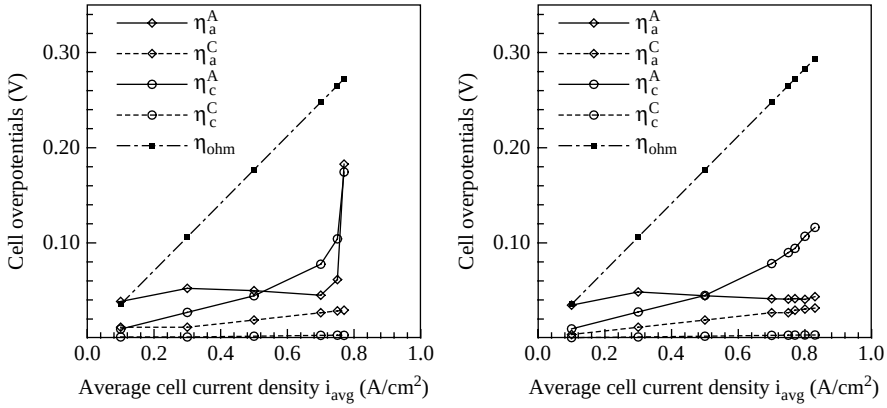

Figure 7.
Anodic and cathodic polarizations as a function of the average current density, when such parameter is kept constant (left) and locally calculated (right) at the catalyst layer

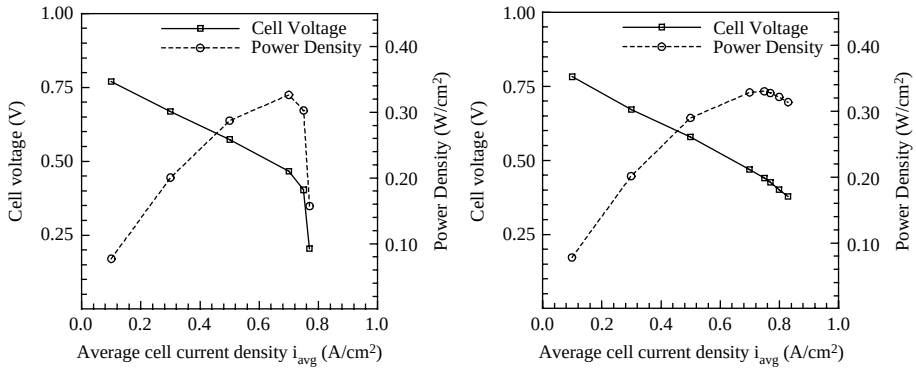

Figure 8.
Power density and operative cell voltage as a function of the average current density, when such parameter is kept constant (left) and locally calculated (right) at the catalyst layer

higher current density values the voltage and power density obtained at the catalyst layer are higher with local current density distribution than one with constant current density assumption.

Figure 9 shows the species convergence histories for hydrogen at the anodic compartment and oxygen at the cathodic compartment, in correspondence of an average current density value $i_{avg} = 0.1$ (left) and $i_{avg} = 0.3\ A/cm^2$ (right), when such parameter is kept constant at the catalyst layer. The convergence histories in Figure 9 are shown keeping the temperature uniform over the domains and consequently give a direct information about the convergence behaviour, since no iteration procedure is required over the domains, as described in Section 0. The presence of very large source terms due to the porous domain, imposed the choice of a very small time step size, kept constant over the computational domain. The residuals in Figure 9 are referred to the first time step residual and to the employed time-step. The figure clearly shows that the number of required iterations increases as the average current density increases. The simulation have been performed on a Intel® Core™2 CPU at 2.40 GHz, 4.0 Gb RAM machine and required 2,050 and 125 s, respectively, for the anodic and the cathodic compartment, when the average current density was $i_{avg} = 0.1\ A/cm^2$. The significant difference between the two computational times clearly depends on the thickness of the two electrodes. Since the species conservation equation is solved explicitly, for different values of the average current density, the CPU time is basically proportional to the number of iterations.

To estimate the temperature distribution in both anodic and cathodic compartments, the fuel and oxidant inlet velocities are set to 2.0 m/s, and the temperature of the air entering the domain is assumed to be 973 K. Figure 10 shows the anodic and cathodic temperature field at a mean current density of $i_{avg} = 0.3\ A/cm^2$. As seen, nearly all the heat generated by fuel cell is removed in the cathodic compartment and maximum temperature in fuel cell is about 1,058 K.

Figure 11 shows the influence of temperature on the cell performance in terms of operative voltage (left) and power density (right). The results have been compared at constant cell temperatures of 923, 1,023 and 1,073 K over the domain. The maximum mean current density produced by the cell is practically the same for 1,023 and 1,073 K, while it is slightly lower at 973 K. This aspect underlines the fact that, within the

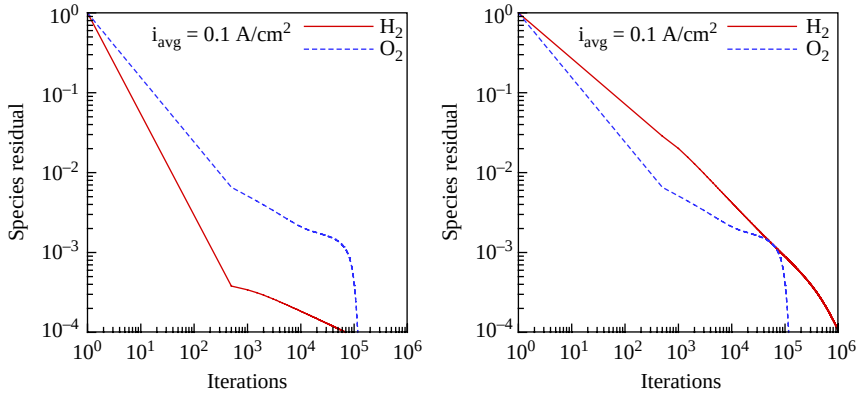

Figure 9.
Convergence histories for hydrogen at the anodic compartment and oxygen for the cathodic compartment at an average current densities $i_{avg} = 0.1\ A/cm^2$ (left) and $i_{avg} = 0.3\ A/cm^2$ (right), when such parameter is kept constant at the catalyst layer

temperature range considered, the dependence of the mass transport phenomena on temperature is less evident than that of the material properties, such as electronic and ionic conductivities.

6. Conclusions

To verify the performance of the CBS code developed for the numerical simulation of fuel cells, the mass and energy transport phenomena in the anodic and cathodic compartments of a planar anode supported SOFC have been simulated. The porous electrodes of the fuel cell have been modelled as saturated porous domains of constant porosity and the generalised model has been employed for the simulation of mass and energy phenomena in free fluid and porous domains. The set of PDEs that describe these phenomena have been numerically solved by employing the semi-implicit version of the CBS algorithm and triangular structured grids. The main conclusions obtained can be summarized as follows:

- the CBS algorithm proposed is general and well-suited for the simulation of fuel cells;
- the results obtained are in good agreement with the numerical and the experimental data available in the literature; and
- allowing local variation in current density improves the solution of SOFC problems.

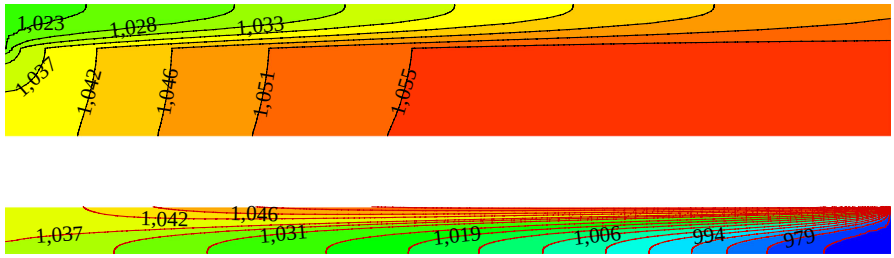

Figure 10.
Temperature distribution at anodic (top) and cathodic (bottom) compartment for an average current density $i_{avg} = 0.3\ A/cm^2$

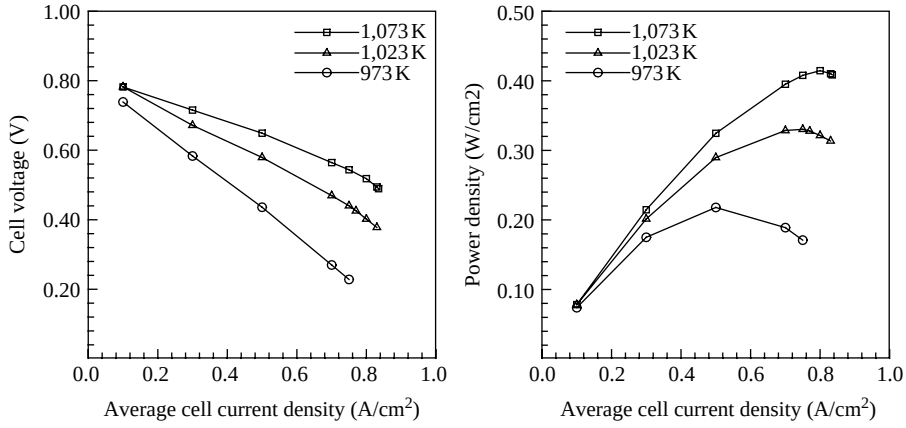

Figure 11.
Cell voltage (left) and cell power density (right) as a function of the mean current density for different value of cell temperatures: 973, 1,023 and 1,073 K, respectively

References

Aguiar, P., Adjiman, C.S. and Brandon, N.P. (2004), "Anode-supported intermediate temperature direct internal reforming solid oxide fuel cell I. Model-based steady-state performance", *Journal of Power Sources*, Vol. 138, pp. 120-36.

Aguiar, P., Adjiman, C.S. and Brandon, N.P. (2005), "Anode-supported intermediate-temperature direct internal reforming solid oxide fuel cell II. Model-based dynamic performance and control", *Journal of Power Sources*, Vol. 147, pp. 136-47.

Autissier, N., Larrian, D., van Herle, J. and Favrat, D. (2004), "CFD simulation tool for solid oxide fuel cells", *Journal of Power Sources*, Vol. 131, pp. 313-9.

Beale, S.B., Lin, Y., Zhubrin, S.V. and Dong, W. (2003), "Computer methods for performance prediction in fuel cells", *Journal of Power Sources*, Vol. 118, pp. 79-85.

Campanari, S. and Iora, P. (2004), "Definition and sensitivity analysis of a finite volume SOFC model for a tubular cell geometry", *Journal of Power Sources*, Vol. 132, pp. 113-26.

Celik, I., Pakalapati, S.R. and Salazar-Villalpando, M.D. (2005), "Theoretical calculation of the electrical potential at the electrode/electrolyte interfaces of solid oxide fuel cells", *Journal of Fuel Cell Science and Technology*, Vol. 2, pp. 238-45.

Chan, S.H. and Xia, Z.T. (2002), "Polarization effects in electrolyte/electrode-supported solid oxide fuel cells", *Journal of Applied Electrochemistry*, Vol. 32, pp. 339-47.

Chan, S.H., Khor, K.A. and Xia, Z.T. (2001), "A complete polarization model of solid oxide fuel cell and its sensitivity to the change of cell component thickness", *Journal of Power Sources*, Vol. 93, pp. 130-40.

Cussler, E.L. (1997), *Diffusion Mass Transfer in Fluid Systems*, Cambridge University Press, New York, NY.

EG&G, S.P. Inc. (2000), *Fuel Cell Handbook*, US Department of Energy Office of Fossil Energy National Energy Technology Laboratory, Morgantown, WV.

Ferguson, J.R., Fiard, J.M. and Herbin, R. (1996), "Three-dimensional numerical simulation for various geometries of solide oxide fuel cells", *Journal of Power Sources*, Vol. 58, pp. 109-22.

Greene, E.S., Chiu, W.K.S. and Medeiros, M.G. (2006), "Mass transfer in graded microstructure solid oxide fuel cell electrodes", *Journal of Power Sources*, Vol. 161, pp. 225-31.

Inui, Y., Urata, A., Ito, N., Nakajima, T. and Tanaka, T. (2006), "Performance simulation of planar SOFC using mixed hydrogen and carbon monoxide gases as fuel", *Energy Conversion and Management*, Vol. 47, pp. 1738-47.

Ji, Y., Yuan, K., Chung, J.N. and Chen, Y-C. (2006), "Effects of transport scale on heat/mass transfer and performance optimization for solid oxide fuel cells", *Journal of Power Sources*, Vol. 161, pp. 380-91.

Khaleel, M.A., Lin, Z., Singh, P., Surdoval, W. and Collin, D. (2004), "A finite element analysis modeling tool for solid oxide fuel cell development: coupled electrochemistry, thermal and flow analysis in MARC", *Journal of Power Sources*, Vol. 130, pp. 136-48.

Larrian, D., van Herle, J. and Favrat, D. (2004), "Generalized model of planar SOFC repeat element for design optimization", *Journal of Power Sources*, Vol. 131, pp. 304-12.

Lehnert, W., Meusinger, J. and Thom, F. (2000), "Modelling of gas transport phenomena in SOFC anodes", *Journal of Power Sources*, Vol. 87, pp. 57-83.

Lewis, R.W., Nithiarasu, P. and Seetharamu, K.N. (2004), *Fundamentals of the Finite Element Method for Heat and Fluid Flow*, Wiley, Chichester.

Li, P.W. and Chyu, M.K. (2003), "Simulation of the chemical/electrochemical reactions and heat/mass transfer for a tubular SOFC in a stack", *Journal of Power Sources*, Vol. 124, pp. 487-98.

Li, P.W. and Chyu, M.K. (2005), "Electrochemical and transport phenomena in solid oxide fuel cells", *Journal of Heat Transfer*, Vol. 127, pp. 1344-62.

Lin, Y. and Beale, S.B. (2006), "Performance predictions in solid oxide fuel cells", *Applied Mathematical Modelling*, Vol. 30, pp. 1485-96.

Lockett, M., Simmons, M.J.H. and Kendall, K. (2004), "CFD to predict temperature profile for scale up of micro-tubular SOFC stacks", *Journal of Power Sources*, Vol. 131, pp. 243-6.

Lu, Y. and Schaefer, L. (2006), "Numerical study of a flat-tube high power density solid oxide fuel cell Part II: cell performance and stack optimization", *Journal of Power Sources*, Vol. 153, pp. 68-75.

Lu, Y., Schaefer, L. and Li, P. (2005), "Numerical Study of a flat-tube high power density solid oxide fuel cell Part I. Heat/mass transfer and fluid flow", *Journal of Power Sources*, Vol. 140, pp. 331-9.

Ma, L., Ingham, D.B., Pourkashanian, M. and Carcadea, E. (2005), "Review of the computational fluid dynamics modeling of fuel cells", *Journal of Fuel Cell Science and Technology*, Vol. 2 No. 4, pp. 246-57.

Massarotti, N., Nithiarasu, P. and Carotenuto, A. (2003), "Microscopic and macroscopic approach for natural convection in enclosures filled with fluid saturated porous medium", *International Journal of Numerical Methods for Heat & Fluid Flow*, Vol. 13 No. 7, pp. 862-86.

Massarotti, N., Nithiarasu, P. and Zienkiewicz, O.C. (2001), "Natural convection in porous medium-fluid interface problems", *International Journal of Numerical Methods for Heat & Fluid Flow*, Vol. 11 No. 5, pp. 473-90.

Massarotti, N., Arpino, F., Lewis, R.W. and Nithiarasu, P. (2006), "Explicit and semi-implicit CBS procedures for incompressible viscous flows", *International Journal for Numerical Methods in Engineering*, Vol. 66, pp. 1618-40.

Nishino, T., Iwai, H. and Suzuki, K. (2006), "Comprehensive numerical modeling and analysis of a cell-based indirect internal reforming tubular SOFC", *Journal of Fuel Cell Science and Technology*, Vol. 3, pp. 33-44.

Nithiarasu, P. (2003), "An efficient artificial compressibility (AC) scheme based on split (CBS) method for incompressible flows", *International Journal for Numerical Methods in Engineering*, Vol. 56, pp. 1815-45.

Nithiarasu, P., Seetharamu, K.N. and Sundararajan, T. (1997), "Natural convective heat transfer in an enclosure filled with fluid saturated variable porosity medium", *International Journal of Heat and Mass Transfer*, Vol. 40, pp. 3955-67.

Nithiarasu, P., Mathur, J.S., Weatherill, N.P. and Morgan, K. (2004), "Three dimensional incompressible flow calculations using the characteristic based split (CBS) scheme", *International Journal for Numerical Methods in Fluids*, Vol. 44, pp. 1207-29.

Perry, R.H., Green, D.W. and Maloney, J.O. (1997), *Perry's Chemical Engineers' Handbook*, 7th ed., McGraw-Hill, New York, NY.

Singhal, S.C. and Kendall, K. (2003), *High-temperature Solid Oxide Fuel Cells: Fundamentals, Design and Applications*, Elsevier Advanced Technology, Kidlington.

Standaert, F., Hemmes, K. and Woudstra, N. (1996), "Analytical fuel cell modeling", *Journal of Power Sources*, Vol. 63, pp. 221-34.

Stiller, C., Thorud, B., Seljebo, S., Mathisen, O., Karoliussen, H. and Bolland, O. (2005), "Finite-volume modeling and hybrid-cycle performance of planar and tubular solid oxide fuel cells", *Journal of Power Sources*, Vol. 141, pp. 227-40.

Sundén, B. and Faghri, M. (2005), *Transport Phenomena in Fuel Cells*, WIT Press, Southampton.

Suwanwarangkul, R., Croiset, E., Entchev, E., Charojrochkul, S., Pritzker, M.D., Fowler, M.W., Douglas, P.L., Chewathanakup, S. and Mahaudom, H. (2006), "Experimental and modeling study of solid oxide fuel cell operating with syngas fuel", *Journal of Power Sources*, Vol. 161, pp. 308-22.

Suzuki, M., Fukagata, K., Shikazono, N. and Kasagi, N. (2005), "Numerical analysis of temperature and potential distributions in planar-type SOFC", paper presented at 6th KSME-JSME Thermal and Fluids Engineering Conference, Jeju.

Vafai, K. (2000), *Handbook of Porous Media*, Marcel Dekker, Inc., New York, NY.

Vafai, K. and Kim, S.J. (1990), "Fluid mechanics of the interface region between a porous medium and a fluid layer – an exact solution", *Int. J. Heat and Fluid Flow*, Vol. 11 No. 3, pp. 254-6.

Whitaker, S. (1961), "Diffusion and dispersion in porous media", *AIChE J.*, Vol. 13, pp. 420-7.

Yakabe, H., Hishinuma, M., Uratani, M., Matsuzaki, Y. and Yasuda, I. (2000), "Evaluation and modeling of performance of anode-supported solid oxide fuel cell", *Journal of Power Sources*, Vol. 86, pp. 423-31.

Yuan, J. and Sundén, B. (2005), "Analysis of intermediate temperature solid oxide fuel cell transport processes and performance", *Journal of Heat Transfer*, Vol. 127, pp. 1380-90.

Zhao, F. and Virkar, A.V. (2005), "Dependence of polarization in anode-supported solid oxide fuel cells on various cell parameters", *Journal of Power Sources*, Vol. 141, pp. 79-95.

Zhu, H. and Kee, R.J. (2003), "A general mathematical model for analyzing the performance of fuel-cell membrane-electrode assemblies", *Journal of Power Sources*, Vol. 117, pp. 61-74.

Zienkiewicz, O.C. and Taylor, R.L. (2000), *The Finite Element Method, 3, Fluid Dynamics*, Butterworth-Heinemann, Oxford.

Zienkiewicz, O.C., Taylor, R.L. and Nithiarasu, P. (2005), *The Finite Element Method for Fluid Dynamics*, Elsevier, Amsterdam.

Corresponding author
F. Arpino can be contacted at: f.arpino@unicas.it